Nanoscale c4nr04510f

1

Cationic carbosilane dendrimers and oligonucleotide binding: an energetic affair

D. Marson, E. Laurini, P. Posocco, M. Fermeglia and S. Pricl*

Molecular simulations individuate the normalized effective free energy of binding as a critical molecular parameter in designing efficient nanovectors for gene delivery.

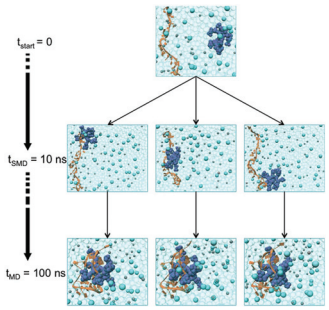

Please check this proof carefully. **Our staff will not read it in detail after you have returned it.**

Translation errors between word-processor files and typesetting systems can occur so the whole proof needs to be read. Please pay particular attention to: tabulated material; equations; numerical data; figures and graphics; and references. If you have not already indicated the corresponding author(s) please mark their name(s) with an asterisk. Please e-mail a list of corrections or the PDF with electronic notes attached – do not change the text within the PDF file or send a revised manuscript. Corrections at this stage should be minor and not involve extensive changes. All corrections must be sent at the same time.

Please bear in mind that minor layout improvements, e.g. in line breaking, table widths and graphic placement, are routinely applied to the final version.

We will publish articles on the web as soon as possible after receiving your corrections; **no late corrections will be made**.

Please return your **final** corrections, where possible within **48 hours** of receipt, by e-mail to: nanoscale@rsc.org

Queries for the attention of the authors

Journal: **Nanoscale**

Paper: **c4nr04510f**

Title: **Cationic carbosilane dendrimers and oligonucleotide binding: an energetic affair**

Editor's queries are marked like this [Q1, Q2, ...], and for your convenience line numbers are indicated like this [5, 10, 15, ...].

Please ensure that all queries are answered when returning your proof corrections so that publication of your article is not delayed.

Query Reference	Query	Remarks
Q1	For your information: You can cite this article before you receive notification of the page numbers by using the following format: (authors), Nanoscale, (year), DOI: 10.1039/c4nr04510f.	
Q2	Please carefully check the spelling of all author names. This is important for the correct indexing and future citation of your article. No late corrections can be made.	

Nanoscale

PAPER

Cationic carbosilane dendrimers and oligonucleotide binding: an energetic affair†

Cite this: DOI: 10.1039/c4nr04510f

D. Marson,‡[a] E. Laurini,‡[a] P. Posocco,[a,b] M. Fermeglia[a] and S. Pricl*[a,b]

Received 6th August 2014,
Accepted 22nd September 2014

DOI: 10.1039/c4nr04510f

www.rsc.org/nanoscale

Generation 2 cationic carbosilane dendrimers hold great promise as internalizing agents for gene therapy as they present low toxicity and retain and internalize the genetic material as an oligonucleotide or siRNA. In this work we carried out a complete *in silico* structural and energetical characterization of the interactions of a set of 2G carbosilane dendrimers, showing different affinity towards two single strand oligonucleotide (ODN) sequences *in vitro*. Our simulations predict that these four dendrimers and the relevant ODN complexes are characterized by similar size and shape, and that the molecule-specific ODN binding ability can be rationalized only by considering a critical molecular design parameter: the normalized effective binding energy $\Delta G_{bind,eff}/N_{eff}$, *i.e.* the performance of each active individual dendrimer branch directly involved in a binding interaction.

Introduction

Molecular nano(bio)technology pertains to either synthetic or natural systems, which have nanoscale dimensions or functioning nanoscale components, ultimately resulting in novel and unique material properties. This branch of science currently occupies a flourishing niche in medicine, known as nanomedicine,[1] particularly within the field of controlled drug/gene delivery. A major, potential benefit of nanomedicine is the design of nanovectors able to deliver their therapeutic cargoes at the required dosage and to the site of lesion, thus maximizing selective effects thereby minimizing toxicity.[2] Truly speaking, the achievement of such ideal nanovectors still remains a sort of chimera, as these nanocarriers and their payloads have to face an aptly organized array of biological barriers along their way to their target site.[3] Efficient nanoparticle transport across biological barriers and within different cell compartments is strongly influenced by the nanovector size, shape, density and surface chemistry and charge. The blend of all these molecular parameters masters the nanovector circulation in the bloodstream, margination, cell membrane adhesion and uptake and, eventually, intracellular trafficking.[4] The overall, multidisciplinary complexity characterizing nanovector design, coupled with the fervent activity in the field, has resulted in a plethora of nanovectors for drug or gene delivery currently investigated being at the pre-clinical or clinical stage.[5]

Gene therapy holds momentous potential for therapeutic intervention in a broad range of genetic maladies, including infectious diseases, gene-related disorders, and cancer. Gene therapy involves intracellular transfer of nucleic acid material to modulate cell functions and responses by expressing exogenous proteins, by silencing a specific gene, or by editing undesirable genomic mutations. Regrettably, most nucleic acids as such not only experience transport problems across the cell membranes but also are subjected to rapid recognition and enzymatic digestion by nucleases. Therefore, appropriate nanovectors able to efficiently allow genetic material to reach the desired population of cells, cross their membranes, discharge the exogenous nucleic acid safely and efficiently to bring out maximum therapeutic effects are highly needed.[6]

Among different molecular systems available for the purpose, dendrimers play the leading role as premiere nanocarriers, especially in gene delivery.[7] Indeed, they provide great gene loading capacity, well-defined physico-chemical properties, and a high degree of molecular diversity that allow extensive modification to help overcome extracellular and intracellular barriers to gene delivery. Specifically, cationic dendrimers such as the renowned poly(amidoamine) dendrimers or PAMAMs, are cationic in nature, in that they contain several amine groups that, according to their nature (primary or tertiary), become protonated at two major physiological pH values (*i.e.*, 7.4 and 5). The interaction of the positively charged dendrimer nanocarriers and the negatively charged nucleic acid results in the spontaneous formation of nanosized complexes – termed polyplexes – in a physiological

[a]*Molecular Simulation Engineering (MOSE) Laboratory, DEA, University of Trieste, Piazzale Europa 1, 34127 Trieste, Italy. E-mail: sabrina.pricl@di3.units.it*
[b]*National Interuniversity Consortium for Material Science and Technology (INSTM), Research Unit MOSE-DEA, University of Trieste, 34127 Trieste, Italy*
†Electronic supplementary information (ESI) available: Additional figures and tables. See DOI: 10.1039/c4nr04510f
‡These authors equally contributed to this work.

environment. The neutral character of these compact nanoobjects helps in protecting the genetic cargo from nuclease attack and ensures stability to the nanovector/cargo ensemble during cellular uptake. Once inside the cell, the ideal dendrimer nanovectors should be able to escape from the endosomal compartment and finally unload their nucleic acid cargo into the cytoplasm. Understanding the critical barriers of gene delivery to cells is a prerequisite for the rational design of efficient nanocarriers. Only with that information in hand, new nanovector systems can be carefully designed and their properties can be fine-tuned to achieve the optimal transfection efficiency along with the desired clinical success.

The recent developments in the fight against the HIV infection have seen the flourishing of new anti-viral drugs which, unfortunately, were all dropped in phase II or III trials due to severe toxicity problems and the insurgence of the drug-resistance phenomenon.[8] Another serious problem faced by HIV antivirals is constituted by the inherent difficulty to reach the target cells (particularly the central nervous system) and their inability to eradicate the latently infected cells. Gene therapy represents a possible, alternative approach to HIV infection treatment, holding promise for a higher efficiency in selectively killing infected cells and cleaning viral reservoirs while abating deleterious side effects.[9] Specifically, short oligonucleotides (ODNs) constitute a class of antisense therapy drugs not only in HIV control but also in the treatment of cancer and other infectious or metabolic dysfunctions.[10] For instance, the 25-base ODN GEM91 binds to the translation initiation site of the *gag* gene of the HIV-1 pathogen of acquired immunodeficiency able to inhibit virus entry/reverse transcription and to reduce steady state viral RNA levels. Similarly, the *rev* gene is involved in the regulated expression of HIV structural genes, as *rev* mutants of HIV-1 are incapable of inducing the synthesis of the viral structural proteins gag, pol, and env, and are therefore replication defective. The antisense ODN referred to as SREV is of sufficient length and complementarity to inhibit the expression of the rev gene and, hence, to halt viral replication.

However, as discussed above, ODN delivery requires an efficient carrier to reach the target cells efficiently and safely. Moreover, by virtue of their high anionic charge, ODNs show a remarkable tendency to bind to serum proteins (*e.g.*, human serum albumin).[11] This results in a lower ODN bioavailability, and hence requires higher ODN doses to reach the expected therapeutic effect. Both non-specific serum protein binding and dose elevation can in turn induce toxic side effects, which ultimately results in an overall lower-than-expected performance of the ODN therapeutic option.

Muñoz-Fernandez *et al.* have recently shown[12] that generation 2 (G2) cationic carbosilane dendrimers, containing ammonium or amine groups in their molecular architecture, could be used as internalizing agents for gene therapy as they present low toxicity, retain and internalize genetic material as oligonucleotides or siRNA. Among this water-soluble carbosilane dendrimer family, compounds 2G-[Si($OCH_2CH_2NMe_3^+I^-$)]$_8$ (**1**), 2G-[Si($OCH_2CH_2NMe_3^+I^-$)$_2$]$_8$ (**2**), 2G-[Si{$O(CH_2)_2N(Me)(CH_2)_2NMe_3^+I^-$}]$_8$ (**3**), and 2G-[Si{$O(CH_2)_2N(Me)_2^+(CH_2)_2NMe_3^+$-$(I^-)_2$}]$_8$ (**4**) (Fig. 1) were thoroughly characterized for their capacity of binding to different ODNs and serum proteins and, most importantly, for their ability to transfect normal primary peripheral blood cells and inhibit HIV-1 replication in the presence of serum.[12]

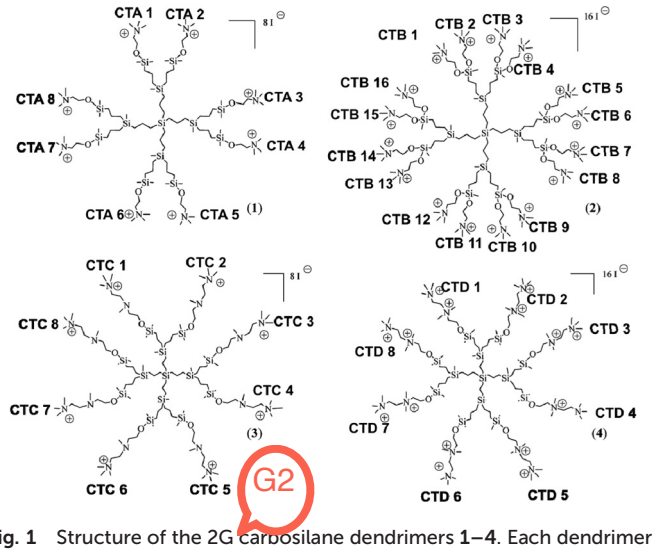

Fig. 1 Structure of the 2G carbosilane dendrimers **1–4**. Each dendrimer branch is labeled for *per residue* binding free energy decomposition purposes (see Results and discussion).

Further studies concerning the use of **1–4** as potential carriers for gene delivery or for other biomedical applications gave encouraging results. Indeed, distinct (but complementary) approaches employed to evaluate membrane integrity, metabolic activity, apoptosis, morphology, and cell movement all revealed that all carbosilane dendrimers are endowed with good toxicity profiles in cell cultures over extended periods.[12] Most importantly, in spite of their low generation number, these carbosilane dendrimers were shown to form complexes with DNA oligonucleotides (ODNs) or even with plasmids at biocompatible doses. In addition, the presence of Si–O bonds in their structure open the way for the use of these molecules as drug delivery systems by exploiting the corresponding hydrolytic process. However, in a dedicated study it was verified that while dendrimers **2–4** could effectively bind GEM91 and SREV (two short ODNs currently employed as antisense antivirals in HIV-1 treatment), dendrimer **1** showed a remarkably low affinity for the nucleic acid with respect to the other members of the molecular family (affinity decreasing in the order **4** ≥ **3** > **2** ≫ **1**).[13] Also, the same study showed that the ODN affinity of all dendrimers **1–4** appeared somewhat higher for the ODN GEM 91 with respect to that exhibited towards the alternative ODN sequence SREV.

Hence, starting from the very first challenge in nanovector design – the efficient interaction of a nanocarrier with its cargo – in this work we aimed at determining the reasons for this differential behavior among these 4 carbosilane dendrimers in binding GEM91 and SREV ODNs. To this goal, we performed a thorough *in silico* characterization of the structural

features of these molecules coupled with an energetic analysis of the corresponding polyplexes.

Interestingly, we found that while all compounds were characterized by similar size and shape, the molecule-specific ODN binding ability could be rationalized considering the normalized effective binding energy $\Delta G_{\mathrm{bind,eff}}/N_{\mathrm{eff}}$, *i.e.* the performance of each active individual dendrimer branch directly involved in a binding interaction.

Simulation methods

Initial model building and refinement

All simulations discussed in this work were carried out using the AMBER14 suite of programs[14] and performed with the GPU version of pmemd, pmemd.cuda, from AMBER14 on the EURORA GPU-CPU supercomputer (CINECA, Bologna, Italy). The four carbosilane dendrimer models were built, parameterized and refined following a consolidated procedure described in detail in our previous work.[15] Briefly, the 3D structure of each dendrimer was built and geometry-optimized using the Antechamber module of AMBER14 consistently with the General Amber Force Field (GAFF).[16] Eventually missing force field terms were derived from quantum mechanical calculations using the GAMESS software[17] and the paramfit of AMBER14. For QM calculations, the MP2/HF/6-31G level of theory was used. van der Waals parameters for Si were taken from the MM3 force field.[18] Partial charges were obtained *via* the resp program implemented in AMBER14. The ODN models for GEM91 (sequence CTC TCG CAC CCA TCT CTC TCC TTC T) and SREV (sequence TCG TCG CTG TCT CCG CTT CTT CTT GCC A) were built with the tleap routine of AMBER14. The force field *ff12SB* was adopted for optimizing the structure of the two ODNs.

The structures of each dendrimer and ODN were immersed in a box of TIP3P water molecules.[19] The dimension of each simulation box was chosen in order to ensure a ~~1 nm~~ 1.5 nm solvation shell around each solute structure. Suitable amounts of Na^+ and Cl^- ions required to achieve solution neutrality and to realize a physiological ionic strength of 0.15 M were added to each system. The resulting hydrated structures were then subjected to an initial Steepest Descent (SD)/Conjugated Gradient (CG) minimization with 5.0 kcal (mol Å^2)$^{-1}$ restraint on the solute (solvent relaxation), followed by another round of CG minimization without restraints in order to eliminate all bad contacts between water molecules and the dendrimer/ODN structure.

Next, each minimized structure was subjected to molecular dynamics (MD) simulations in the canonical ensemble (constant volume/constant temperature, or NVT). During this 100 ps MD, each system was gradually heated and relaxed to 300 K. The SHAKE algorithm[20] was applied to all covalent bonds involving hydrogen atoms. An integration time step of 2 fs was adopted together with the Langevin thermostat for temperature regulation (collision frequency = 2.0 ps^{-1}).[21] The final heating step was followed by 50 ns of MD equilibration in the isochoric/isothermal (NPT) ensemble. Pressure control was exerted by coupling the system to a Berendsen barostat (pressure relaxation time 2 ps).[22] The particle Mesh Ewald (PME)[23] method was used to treat long-range electrostatic interactions under periodic conditions with a direct space cut-off of 10 Å. A frame from each equilibrated MD trajectory of the dendrimers and ODN was extracted to build different carrier/nucleic acid complex initial configurations.

For the construction of the dendrimer/ODN complex models, we resorted to a novel procedure based on Steered Molecular Dynamics (SMD) simulations.[24] Specifically, the equilibrated dendrimer and ODN structures extracted from the corresponding equilibrated MD simulations were placed 60 Å away from each other in a solvated box. Next, the dendrimer was pulled close to its target using a force of 50 kcal (mol Å^2)$^{-1}$ and a velocity of 5 Å ns^{-1}. The phosphorous atoms of the ODN were forced in their position by applying a weak restraint of 0.5 kcal (mol Å^2)$^{-1}$. This allowed avoiding substantial deformation of the ODN during the dendrimer pulling process. Once the dendrimer reached the proximity of the ODN (*i.e.*, distance between the dendrimer and the ODN center of mass approximately 12 Å), this restraint was released and both molecules were allowed to move to reach the final complex configuration.

Each resulting dendrimer/ODN complex was again equilibrated for 50 ns of equilibration in the NPT ensemble and, starting from the last equilibrated frame, we next performed further 50 ns of simulation in an NVT ensemble for data collection and analysis.

Structural analysis

The structural analysis of the dendrimers *per se* and in complex with the two ODNs was performed using the *cpptraj* program of AMBER14. Further calculations were carried out using in-house developed python scripts. If not differently stated, all structural data discussed represent values averaged over the last 40 ns of the production runs, with MD trajectory snapshots taken every 40 ps.

Free energy of binding

The dendrimer/ODN free energy of binding ΔG_{bind} was derived following our thoroughly validated methodology[15] based on the Molecular Mechanics/Poisson Boltzmann Surface Area (MM/PBSA) approach.[25] This computational technique employs snapshots taken from MD trajectories to estimate the average interaction energies based on the solute molecular mechanics internal energy (ΔE_{MM}) and solvation energy (ΔG_{solv}), the latter obtained *via* Poisson–Boltzmann (PB) continuum solvent calculations. According to MM/PBSA, the overall binding energy ΔG_{bind} is given by the difference in energy between the dendrimer/ODN complex and the individual dendrimer and ODN:

$$\Delta G_{\mathrm{bind}} = \Delta G_{\mathrm{complex}} - \Delta G_{\mathrm{dendrimer}} - \Delta G_{\mathrm{ODN}} \quad (1)$$

where

$$\Delta G_{\text{bind}} = \Delta E_{\text{MM}} + \Delta G_{\text{solv}} - T\Delta S \quad (2)$$

$$\Delta E_{\text{MM}} = \Delta E_{\text{int}} + \Delta E_{\text{vdW}} + \Delta E_{\text{ele}} \quad (3)$$

$$\Delta E_{\text{int}} = \Delta E_{\text{bond}} + \Delta E_{\text{angle}} + \Delta E_{\text{tors}} \quad (4)$$

$$\Delta G_{\text{solv}} = \Delta G_{\text{PB}} + \Delta G_{\text{np}} \quad (5)$$

ΔE_{MM} is the system change in molecular mechanical energy upon binding, which consists of internal energy ΔE_{int} (due to bonds, angles, and dihedral angle variations), electrostatic energy (ΔE_{ele}) and van der Waals (ΔE_{vdW}) contributions. The solvation energy term ΔG_{solv} consists of two components: the electrostatic term ΔG_{PB} and the nonpolar term ΔG_{np}. ΔG_{PB} is obtained by solving the Poisson–Boltzmann equation while ΔG_{np} can be obtained *via* the semi-empirical expression: $\Delta G_{\text{np}} = \gamma \times \text{SASA} + \beta$, in which SASA is the solvent accessible surface area of the molecule, γ is the surface tension parameter (0.00542 kcal Å^{-2} mol^{-1}), and β = 0.92 kcal mol^{-1}. Finally, the entropic contribution $-T\Delta S$ is calculated *via* normal mode of harmonic frequencies obtained from a subset of minimized snapshots taken from the corresponding MD trajectories.

In this work, we adopted the so-called "multi-trajectory approach", wherein the bound and unbound states of the dendrimers and the ODNs are simulated separately, in contrast to the widely adopted "single trajectory" procedure. This choice was dictated by the necessity for effectively sampling the unbound state of the dendrimer and the ODN for free energy calculations. The single trajectory method is indeed appropriate for those systems in which the molecules do not undergo substantial conformational changes upon binding, which is not the case for the compounds of interest in the present work.

The analysis of the energy of interactions between the dendrimers and the ODNs was accomplished with the MMPBSA.py script implemented in AmberTools14. Energy values were averaged over 200 frames taken during an equally spaced time interval during the last 15 ns of the MD production steps. Normal mode analysis was carried out on a subset of 15 minimized MD snapshots evenly extracted from the relevant trajectory time frame used for energy calculations.

Finally, the effective number of charges involved in binding, and the corresponding effective free energy of binding values were obtained performing a *per residue* binding free energy decomposition exploiting the MD trajectories of each given dendrimer/ODN ensemble.[26] This analysis was carried out using the MM/GBSA approach,[27] and was based on the same snapshots used in the binding free energy calculations.

Results and discussion

Structural aspects of G2 carbosilane dendrimers 1–4

To characterize the structure and properties of these dendrimers, we have selected the following quantities: (i) radius of gyration R_g; (ii) solvent accessible surface area SASA; (iii) shape tensor S; (iv) molecular asphericity δ; and (v) monomer density distribution $\rho(r)$.

Table 1 Number of atoms N (–), radius of gyration R_g (Å), asphericity δ (–), and solvent accessible surface area *SASA* (Å^2) of dendrimers **1–4**

	N	R_g	δ	*SASA*
1	361	9.07 ± 0.21	0.0126	1910 ± 87
2	489	10.39 ± 0.13	0.0096	2699 ± 76
3	449	9.92 ± 0.28	0.0174	2288 ± 82
4	481	10.62 ± 0.25	0.0103	2555 ± 72

A parameter that provides a quantitative characterization of the size of a molecule is the radius of gyration R_g. For a given dendrimer of N atoms, the mean-square radius of gyration is defined as

$$\langle R_g{}^2 \rangle = \left(\frac{1}{M}\right) \left\langle \left[\sum_{i=1}^{N} m_i [r_i - R]^2 \right] \right\rangle \quad (6)$$

where R is the center of mass of the dendrimer, r_i and m_i are the position and mass of the i^{th} atom, and M is the total mass of the dendrimer.

Table 1 lists the values of R_g obtained from equilibrated MD trajectories of **1–4** in water at 0.15 mM NaCl. As we see, dendrimers **1** and **3**, both characterized by 8 positive charges on their surface (Fig. 1), have similar values of R_g. (9.07 and 9.92 Å, Table 1). As somewhat expected, the two other dendrimers **2** and **4** bearing 16 positive charges on their scaffolds have larger dimensions with respect to their less charged counterparts (10.39 and 10.62 Å, Table 1). Interestingly, however, the different molecular architecture of **2** and **4** (containing 8 groups of single and doubly methylated outer fragments, respectively, Fig. 1) does not result in a significant difference in their R_g values.

Considering the lowest generations of the most popular dendrimer family, the ethylenediamine-core (EDA) poly(amidoamine)s or PAMAMs, as a proof-of-concept for comparison, it is interesting to observe that the literature R_g values for the G1-PAMAM, with 8 positively charged terminal groups at pH 7.4, fall in the interval 7.5–9.9 Å, while those for the G2-PAMAM, with 16 charged terminal groups at physiological pH range from 9.2 to 13.6 Å.[28] Notwithstanding the well-known literature controversy about R_g values for PAMAM dendrimers, we are tempted to observe that, on average, the calculated R_g values of all G2 carbosilane dendrimers **1–4** fall in an intermediate range of dimensions between G1- and G2-PAMAMs. The comparison between G2 carbosilanes **2** and **4**, and the G2-PAMAM is straightforward: both G2 dendrimer families feature 16 positive charges in their outer shell and are characterized by similar values of atom numbers (N) and solvent accessible surface areas (SASA). Indeed, N = 489, 481, and 532 and SASA = 2699, 2555, and 2333 Å^2 for **2**, **4**, and G2-PAMAM, respectively (Table 1 and ref. 28). The results for the carbosilane dendrimers **1** and **3** can be rationalized by considering that these two molecules do bear the same charge of G1-

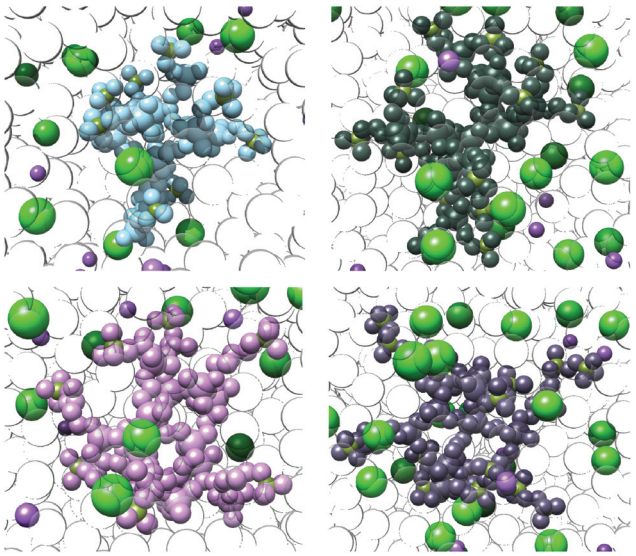

Fig. 2 Zoomed view of equlibrated MD snapshots of G2 carbosilane dendrimers **1** (top left), **2** (top right), **3** (bottom left), and **4** (bottom right). In all panels, the dendrimers are shown as colored sticks (**1**, light blue; **2**, dark sea green, **3**, plum; **4**, dark lavender), water is portrayed as light gray transparent spheres, and some Na^+ and Cl^- ions are depicted as purple and green spheres, respectively. Hydrogen atoms are omitted for clarity.

PAMAM (+8) but, being a generation 2, they are also characterized by a number of atoms and, accordingly, a solvent accessible surface area quite larger than those pertaining to G1-PAMAM. In fact, while N = 361 and 489 for **1** and **3**, respectively (Table 1), the N value for a EDA-core G1 PAMAM is 236; in line with this, the calculated SASA for G1 PAMAM is quite smaller (1341 Å)[28] than the corresponding SASA values obtained for **1** and **3** (1910 and 2288 $Å^2$, Table 1). This evidence supports the fact that the R_g values of **1** and **3** lie in the upper limit of the G1-PAMAM interval.

Concerning the shape of G2 carbosilane dendrimers **1–4**, the first, qualitative clue is provided by Fig. 2, showing snapshots extracted from the corresponding equilibrated MD trajectories. From these images we see that, at variance with the reference G2 PAMAMs that are characterized by a highly asymmetrical conformation,[28] all **1–4** molecules are characterized by a symmetrical, nearly spherical shape.

A quantitative support to this qualitative assertion is afforded by the shape tensor $\boldsymbol{S}$, describing the molecular mass distribution as

$$\boldsymbol{S} = \sum_{i=1}^{N} m_i \left[(r_j r_i)\mathbf{1}_3 - (r_j r_i^{\mathrm{T}}) \right] \tag{7}$$

where r_i is the position of the i^{th} atom with respect to the center of mass of the molecule and $\mathbf{1}_3$ is the unitary matrix of dimension 3. Transformation to the principal axis system diagonalizes $\boldsymbol{S}$ (S = diag(I_x,I_y,I_z)), and the three eigenvalues of $\boldsymbol{S}$ (I_z, I_y, and I_x, sorted in the descending order) are the principal moments of inertia of the equivalent ellipsoid. The

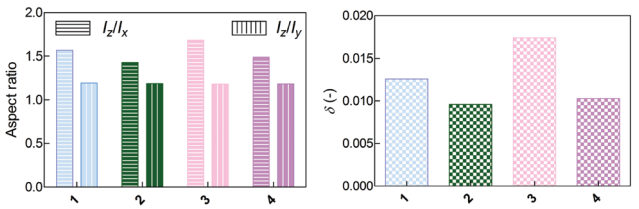

Fig. 3 Moment of inertia-based aspect ratios (left) and asphericity parameter δ (right) for the G2 carbosilane dendrimers **1–4** generated from the corresponding equilibrated MD trajectories.

first invariant of $\boldsymbol{S}$ gives the squared radius of gyration (Tr S = $I_x + I_y + I_z = R_g^2$) while the second invariant shape descriptor, or the asphericity δ, reflects the deviation from a spherical shape of a molecular conformation:[29]

$$\delta = 1 - 3\frac{\langle I_2 \rangle}{\langle I_1^2 \rangle} \tag{8}$$

where I_1 and I_2 refer to the first and second invariants of the shape tensor:

$$I_1 = I_x + I_y + I_z \tag{9}$$

$$I_2 = I_x I_y + I_y I_z + I_x I_z \tag{10}$$

Fig. 3 shows the moment of inertia-based molecular aspect ratios and the asphericity parameter δ for the G2 carbosilane dendrimers **1–4** as obtained from the corresponding equilibrated MD trajectories. We see that for all dendrimers both aspect ratios I_z/I_x and I_z/I_y are in the range 1.0–1.7, indicating that these molecules are strongly compact spheroids independent of their charge (+8/+16). In keeping with this, the asphericity parameter δ values are all quite small and close to zero (Fig. 3 and Table 1 for numerical values), confirming the spherical character of these dendrimer conformations.

At variance with EDA-core PAMAMs, for which lower generation molecules (G1–G3) tend to assume highly asymmetrical shapes whereas higher generations (G5–G7) become nearly spherical, G4 being a transition between the two forms,[28] the carbosilane dendrimers **1–4** already attain a spherical distribution of mass at G2. Aside from eventual small differences in their branch flexibility and/or hydrophilicity, this difference can be essentially attributed to the geometry of the core. Indeed, we know that the size, shape, and initiator-core multiplicity N_c exert a dramatic influence on the ultimate critical molecular design parameters (CMDPs)[30] of a dendrimer. Thus, although for both dendrimer families N_c = 4, the initiator-core for the G2 carbosilane dendrimers consists of a single, Si atom from which the four branches emanate directly and radially in space. In contrast, in the case of the EDA-based PAMAMs the core consists of a small, flexible, 4 atom-long chain, to which the dendrons are tethered and extend from its extremes. As the initiator-core is a dendrimer primary template, these differences are transcribed and displayed through the dendrimer development; thus, the carbosilane dendrimers **1–4** are already spherical at lower generations while higher generation

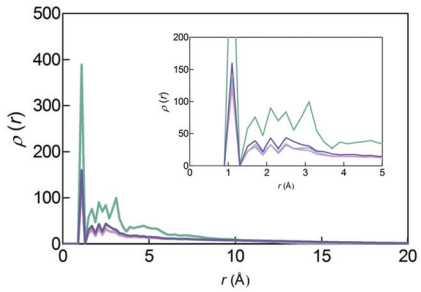

Fig. 4 Monomer density distribution $\rho(r)$ for the G2 carbosilane dendrimers **1–4**. Color legend: **1**, light blue; **2**, dark sea green; **3**, plum; **4**, dark lavender.

numbers are required for EDA-core PAMAMs to fold into a sphere.

The average radial monomer density $\rho(r)$ can provide information about the internal structure of the simulated dendrimers. $\rho(r)$ can be defined as the number of atoms whose center of mass is located within a spherical shell of radius r and thickness Δr. Accordingly, integration over r yields the total number of atoms $N(R)$ as

$$N(R) = 4\pi \int_0^R r^2 \rho(r) \mathrm{d}r \qquad (11)$$

Fig. 4 shows the overall radial density profiles for the G2 carbosilane dendrimers **1–4**, calculated taking the origin as the center of mass of the dendrimer (see also Fig. SI1† for details). As we see, all dendrimers are characterized by almost superimposable profiles indicative of a rather uniform space filling: the curves spike at small R, and then almost monotonically decrease, the width of the tail zone being again very similar for all 4 dendrimers. This is a further confirmation of the fact that the same branching pattern and, above all, the presence of a tetravalent Si atom as the common initiator-core for these G2 carbosilane dendrimers dictate the overall, similar conformation of these molecules.

Complexation of G2 carbosilane dendrimers with ODNs

Given the similarities in size and shape shared by G2 carbosilanes **1–4**, in order to explain the difference in binding affinities of the four dendrimers for the two ODN sequences GEM91 and SREV we went on and performed MD simulations of the relevant complexes. At variance with other studies reported in the literature, in this work we adopted an alternative approach based on a combination of steered molecular dynamics (SMDs) and classical MD experiments to determine the initial geometries of each dendrimer/ODN complex. Specifically, starting from a common initial configuration, each dendrimer was guided towards three different regions of the ODN (*i.e.*, the two ends and the center of the ODN sequence) by SMD simulations and, once a distance of approximately 12 Å was achieved, each configuration was allowed to evolve to equilibrium by classical MD simulation runs. Fig. 5 illustrated this procedure taking dendrimer **4** and

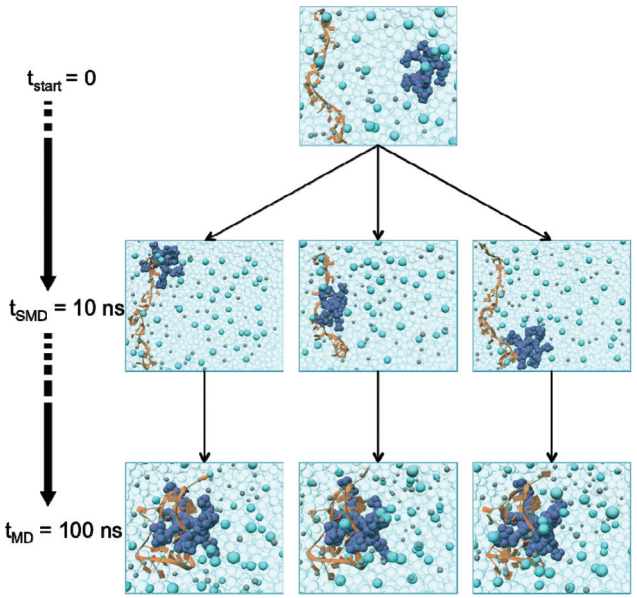

Fig. 5 Coupling steered molecular dynamics (SMD) and classical MD simulations to mimic the binding process of dendrimer **4** to the ODN GEM91 (see the text for more details). The dendrimer is portrayed as dark lavender spheres while the ODN strand is represented as an orange ribbon. Water and oxygen atoms are shown as transparent aqua spheres, whereas some Na^+ and Cl^- ions are portrayed as gray and cyan spheres, respectively.

the ODN GEM91 as examples. As can be seen from the images in Fig. 5, independently of the initial binding region the ODN is completely wrapped around the dendrimer and the resulting complexes become virtually indistinguishable at the end of each combined MD process. Analogous results were obtained with all dendrimers and with both ODN sequences.

To quantitatively substantiate the equivalence of the three final structures, we compared the distance between the dendrimer/ODN centers of mass (COM) and the radial monomer distributions $\rho(r)$ of the corresponding complexes, as illustrated in Fig. 6 taking again the complex between **4** and GEM91 as an example. The left panel in Fig. 6 shows that, when the dendrimer/ODN binding process is started from a configuration where, at the end of the SMD part, the dendrimer docks into the center of the nucleic acid single strand, a very short time is required for the ODNs to wrap around the dendrimers; accordingly, the COM distance of the relevant complexes readily reach their equilibrium value (7 Å on average, Fig. 6). When the dendrimers bind to either end of the ODN sequences, the nucleic acid needs to overcome larger energetic and entropic barriers in order to fold before it can find its wrapping around the dendrimer surface.

This more complex folding pathway clearly requires longer times, but in the end the COM distances between dendrimers and ODNs do converge to the same equilibrium value (Fig. 6). Also, rather importantly, the degree of ODN strand/dendrimer compenetration, defined as the integral of the area shared by the dendrimer and ODN $\rho(r)$ curves (see the right panel of

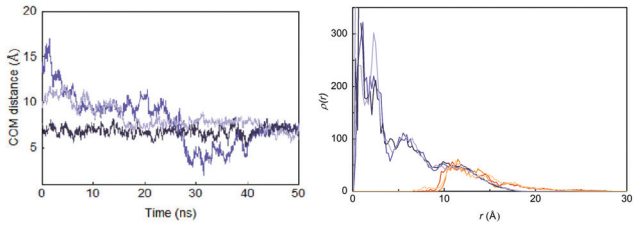

Fig. 6 (left) Center of mass (COM) distance between dendrimer **4** and the ODN GEM91 as a function of time for the three, different initial binding positions: light and medium lavender, dendrimer initially bound by SMD at the ends of the ODN strand; dark lavender, dendrimer initially bound by SMD in the middle of the ODN sequence. (right) Radial monomer distribution of dendrimer **4** and GEM91 of the three final, equilibrated complex structures. Color legend: light lavender (**4**)/light orange (ODN) and medium lavender (**4**)/medium orange (ODN): MD equilibrated configuration obtained from the dendrimer initially bound by SMD at the ends of the ODN strand; dark lavender (**4**)/dark orange (ODN): MD equilibrated configuration obtained from the dendrimer initially bound by SMD in the middle of the ODN strand.

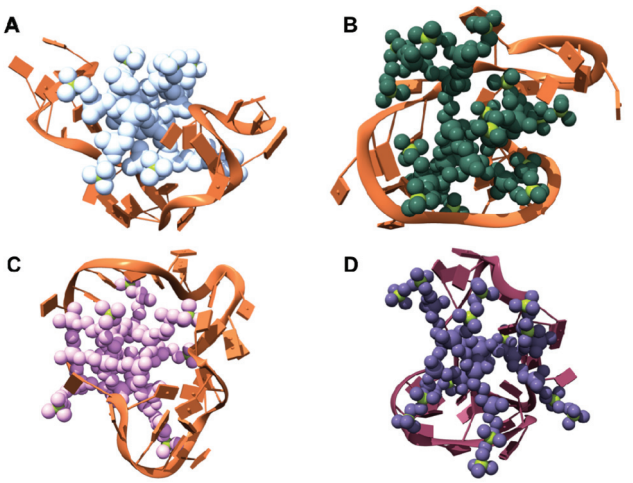

Fig. 7 Equilibrated MD snapshots of dendrimers **1–4** in complex with the ODN GEM91. Dendrimers **1** (A), **2** (B), **3** (C), and **4** (D) are depicted as light sky blue, dark sea green, plum, and dark lavender sticks and balls, respectively, with terminally charged amine groups highlighted in green. The GEM91 sequence is portrayed as an orange ribbon. Water and ions are omitted for clarity.

Fig. 6), is very similar in the three cases of Fig. 5, being equal to 72.1%, 75.5%, and 72.9%, respectively.

Conclusive proof of the equivalence of the dendrimer/ODN final complex structures produced by the combined SMD/MD approach can be found in the corresponding values of the free energy of binding ΔG_{bind}, as calculated *via* the MM/PBSA ansatz. Referring again to the GEM91/**4** assembly as an example (see Table SI1† for all other cases), the ΔG_{bind} values calculated for the two equilibrated complex structures having the dendrimer initial position at one extreme of the ODN strand (*e.g.*, the bottom panel in Fig. 5, right and left images) are -53.4 ± 4.6 kcal mol^{-1} and -53.3 ± 5.1 kcal mol^{-1}, respectively, while for the complex originating from the assembly featuring the dendrimer centrally with respect to the ODN strand (bottom panel, central in Fig. 5 central image) $\Delta G_{bind} = -54.9 \pm 5.0$ kcal mol^{-1}. It is evident that, also from an energetic standpoint, the three structures are indeed comparable, the difference in the affinity between the dendrimer and ODN being within the relevant ΔG_{bind} standard deviation intervals. Of note, utterly similar results are obtained for all other dendrimers, both in complex with GEM91 and SREV.

Given the structural equivalence of the three, final equilibrated structures of each dendrimer/ODN complex, all the remaining discussions will be focused on one single structure only, *i.e.* the one generated from SMD experiments placing the dendrimer central to the nucleic acid strand.

Structural aspects of the complexes

Fig. 7 and SI2† offer a zoomed view of the equilibrated structures of each ODN/dendrimer conformation.

From these images we can observe how, independently of the positive charge content of the dendrimers, the ODN not only wraps around them but we also see a significant compenetration of the two molecular entities. To quantify this pictorial evidence, Table 2 lists the values of some important structural parameters extracted from the analysis of the equilibrated MD trajectory of all dendrimer/ODN complexes.

Table 2 Radius of gyration R_g (Å), asphericity δ (–), interface area between the dendrimer and ODN INT (Å^2), and the average number of contacts between the dendrimer positively charged nitrogen atoms and the ODN negatively charged oxygen atoms N_c (–) for dendrimers **1–4** in complex with GEM91 and SREV ODNs

	GEM91			
	R_g	δ	INT	N_c
1	9.16 ± 0.11	0.0128	233 ± 32	6.1 ± 0.2
2	10.46 ± 0.12	0.0099	709 ± 46	9.7 ± 0.2
3	9.99 ± 0.10	0.0185	1723 ± 53	15.2 ± 0.3
4	10.71 ± 0.11	0.0107	1953 ± 62	17.2 ± 0.3
	SREV			
	R_g	δ	INT	N_c
1	9.13 ± 0.12	0.0150	194 ± 29	5.7 ± 0.3
2	10.42 ± 0.10	0.0102	515 ± 38	7.9 ± 0.2
3	9.87 ± 0.11	0.0188	1762 ± 51	15.5 ± 0.4
4	10.70 ± 0.11	0.0108	1878 ± 66	15.5 ± 0.3

A swift survey of the values shown in Table 2 reveals that the G2 carbosilane dendrimers **1–4** do not change the size and shape upon binding to the ODNs. Indeed, both R_g and δ values for the dendrimers in the complexes are virtually indistinguishable from those of the dendrimers alone (Tables 1 and 2, see also Fig. SI3†). In line with this, Fig. 8 shows the time evolution of the radius of gyration R_g of the ODN GEM91 in complex with dendrimers **1–4** as an example.

However, some differences between the dendrimer complexes with GEM91 and those involving SREV begin to appear. First, the values of the dendrimer/ODN interface areas (INT)

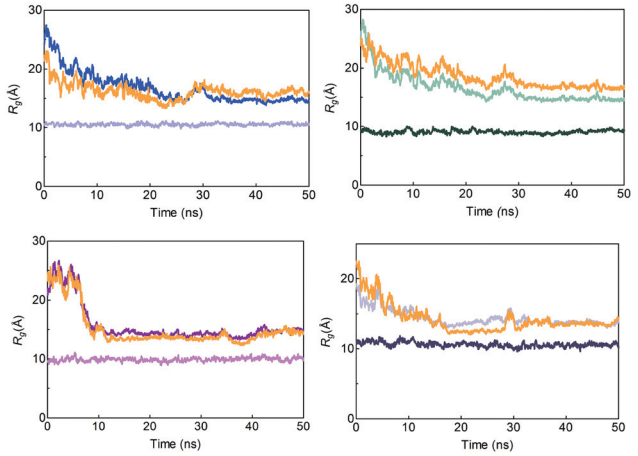

Fig. 8 Evolution of the radius of gyration R_g of the ODN GEM91, the dendrimers **1–4**, and the relevant complexes showing the shape invariance of the dendrimers and the conformational adaptation of the ODN upon binding. (top left) **1**, light blue; ODN GEM91, orange, complex, dark blue; (top right) **2**, dark sea green, ODN GEM91, orange, complex, light sea green; (bottom left) **3**, plum; ODN GEM91, orange; complex, purple; (bottom right) **4**, dark lavender, ODN GEM91 orange, complex, light lavender.

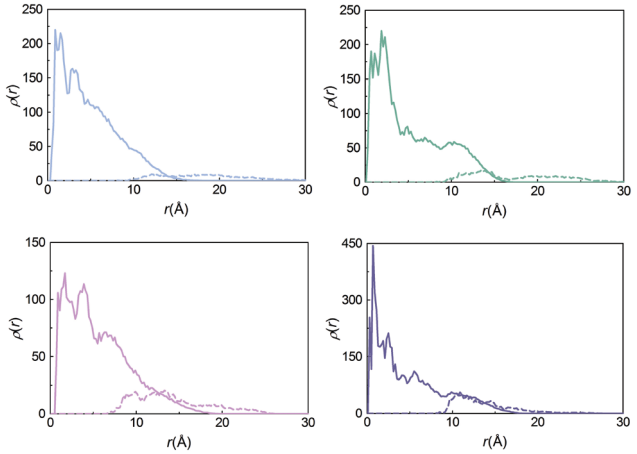

Fig. 9 Density distribution $\rho(r)$ for the dendrimers **1–4** and the ODN GEM91 in the relevant complexes. Top left, **1**; top right, **2**; bottom left, **3**; bottom right **4**. Dendrimer and ODN curves are represented by continuous and broken lines, respectively.

Table 3 Radius of gyration R_g (Å) of the two ODNs GEM91 and SREV wrapped around the dendrimers **1–4** and of the relevant complexes

	GEM91			SREV	
	ODN	Complex		ODN	Complex
1	15.83 ± 0.55	15.44 ± 0.49	**1**	17.28 ± 0.28	15.69 ± 0.21
2	15.57 ± 0.36	15.00 ± 0.27	**2**	16.12 ± 0.23	15.50 ± 0.20
3	13.87 ± 0.25	14.34 ± 0.50	**3**	15.20 ± 0.19	14.44 ± 0.17
4	13.71 ± 0.50	13.98 ± 0.30	**4**	14.95 ± 0.25	14.20 ± 0.20

within the complexes (Table 2) are different between the different dendrimers and, for a given dendrimer, between GEM91 and SREV.

Specifically, for both ODNs *INT* monotonically increases in passing from **1** to **4**, although the difference in INT values progressively levels off between dendrimers **3** and **4**. Also, the INT values are lower for all dendrimers in complex with SREV with respect to the GEM91 complex counterparts (Table 2). In keeping with this, also the number of contacts between the positively charged nitrogen atoms on the dendrimers and the negatively charged oxygen atoms of the ODN phosphate groups N_c follows the same trend: N_c increases from **1** to **4** and is larger (on average) for GEM91 with respect to SREV (Table 2). In keeping with these results, the values of R_g for the GEM91/dendrimer complexes are slightly lower than those of the SREV counterparts (Table 3), suggesting a smaller degree of penetration and, hence, somewhat weaker interactions between the G2 carbosilane dendrimers and the SREV strand.

Considering the monomer density distribution of the dendrimer/ODN complexes yields further information on the structural features of these supermolecular assemblies. For the purpose of discussion, Fig. 9 shows these distributions for dendrimer **4** in complex with ODN GEM91.

Upon binding, the curve of the ODN single strand shows the maximum in the location of the dendrimer terminal groups, which roughly corresponds to the radius of gyration of the dendrimers. Also, we distinctly see a substantial penetration of the ODN within the dendrimer structure. However, considering again the degree of compenetration of the ODN strand and the dendrimer, differences among the diverse dendrimers and between the two strands can be detected. In fact, not only this parameter increases in going from dendrimer **1** to dendrimer **4** for a given ODN, but it also slightly decreases in passing from GEM91 to SREV (in the order: 37.6% (**1**), 55.0% (**2**), 72.0% (**3**), and 75.7% (**4**) for GEM91 and 32.1% (**1**), 47.5% (**2**), 65.2% (**3**), and 73.7% (**4**) for SREV, respectively).

These pieces of evidence could be taken as the first, rough indication that the interactions of the dendrimers with a given ODN decrease in the order **4** ≥ **3** > **2** > **1** and that, for a given dendrimer, more favorable interactions characterize the complex with the ODN GEM91 than the assembly with ODN SREV.

Energetical aspects of ODN/dendrimer binding

To substantiate these seemingly different binding interactions among the G2 carbosilane dendrimers **1–4** and the two single strand nucleotide sequences GEM91 and SREV, we next processed the data collected during equilibrated MD simulations of the single molecular species and the relevant complexes in the framework of the MM/PBSA theory. Specifically, we assessed the effective free energy of binding $\Delta G_{bind,eff}$, that is the contribution to binding yielded by the dendrimer branches in constant and productive contact with the nucleic acid fragment, as shown in Table 4 (see also Table SI3†). To estimate $\Delta G_{bind,eff}$ for each dendrimer/ODN complex, all branches of dendrimers **1–4** involved in ODN binding (N_{eff}, Table 4) were

Table 4 Predicted number of effective dendrimer branches N_{eff} (–), effective free energy of binding $\Delta G_{bind,eff}$ (kcal mol^{-1}), and normalized effective free energy of binding $\Delta G_{bind,eff}/N_{eff}$ (kcal mol^{-1}) for dendrimers **1–4** in complex with the two ODN sequences GEM91 and SREV

	GEM91		
	N_{eff}	$\Delta G_{bind,eff}$	$\Delta G_{bind,eff}/N_{eff}$
1	6	−11.9 ± 1.4	−2.0 ± 0.2
2	9	−23.9 ± 2.1	−2.7 ± 0.2
3	8	−34.6 ± 2.9	−4.3 ± 0.4
4	8	−45.9 ± 3.6	−5.7 ± 0.5
	SREV		
	N_{eff}	$\Delta G_{bind,eff}$	$\Delta G_{bind,eff}/N_{eff}$
1	6	−11.3 ± 0.8	−1.9 ± 0.1
2	9	−22.0 ± 2.0	−2.4 ± 0.2
3	8	−32.2 ± 4.2	−4.0 ± 0.5
4	8	−43.1 ± 4.3	−5.4 ± 0.5

Table 5 The type and number of intermolecular interactions between dendrimers **1–4** and the two ODN sequences GEM91 and SREV as detected in the corresponding equilibrated MD trajectories

	GEM		
	Salt bridge	H-bond	π–cation
1	6	—	—
2	9	—	—
3	8	8	—
4	8	3	5
	SREV		
	Salt bridge	H-bond	π–cation
1	6	—	—
2	9	—	—
3	8	8	—
4	8	4	4

precisely identified (see Fig. 1) and their individual contribution towards the overall binding energy estimated *via* a *per residue* deconvolution of the binding free energy (Table SI2†). The first, interesting finding of this analysis concerns a number of dendrimer branches efficiently involved in binding the two ODNs. Indeed, in both ODN complexes the G2 carbosilane dendrimer **1** has the smallest number of branches in contact with the nucleic acid (N_{eff} = 6), while the remaining three dendrimers have more branches (8/9, Table 4) effectively involved in ODN binding. Contextually, $\Delta G_{bind,eff}$ is larger (*i.e.*, more negative and, hence, more favorable) for dendrimers **2–4** with respect to dendrimer **1**, in both series of complexes (Table 4). Normalizing $\Delta G_{bind,eff}$ by N_{eff} yields the performance of the different dendrimers in using each active individual branch directly involved in a binding interaction ($\Delta G_{bind,eff}/N_{eff}$, Table 4). As we see, $\Delta G_{bind,eff}/N_{eff}$ increases substantially in passing from dendrimer **1** to dendrimer **4** for both ODN complexes, the difference between dendrimers leveling off between dendrimers **3** and **4**. Also, from data in Table 1 a small efficiency in binding GEM91 with respect to SREV can be envisaged.

The differential efficacy in binding the ODNs shown by the four G2 carbosilane dendrimers finds its molecular roots in the diverse number and type of interaction each dendrimer branch is able to establish with the nucleic acid. As shown in Table 5, independently of their structural details and their charge, all dendrimers exploit a conspicuous number of salt bridges between the terminal, positively charged nitrogen of the dendrimer atoms and the negatively charged oxygens of the ODN phosphate groups (see, for instance, Fig. 10, panels A and B).

However, the presence of a second N atom in the dendrimer branches as in dendrimers **3** and **4** allows for further intermolecular interactions, the nature and number of which depend on that atom being electrically neutral (**3**) or positively charged (**4**). Indeed, a number of H-bonds are generated within each ODN/dendrimer complex in the case of **3** (Table 5 and

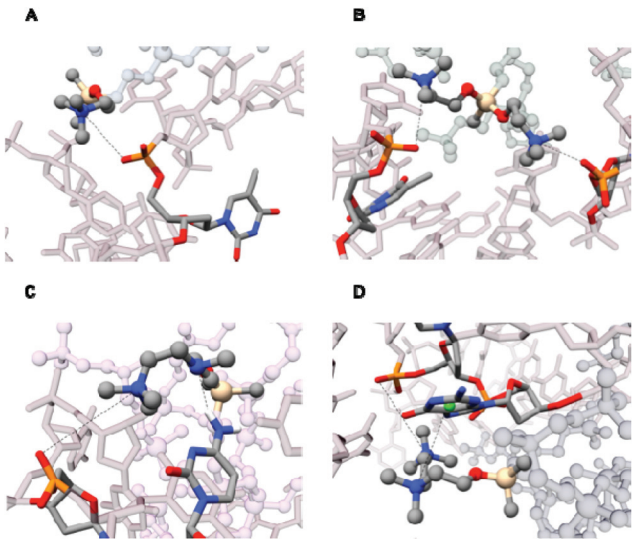

Fig. 10 Zoomed view of the different intermolecular interactions between the G2 carbosilane dendrimers **1–4** and the ODN GEM91, as detected in the equilibrate portion of the corresponding MD trajectories. Dendrimers **1** (A), **2** (B), **3** (C), and **4** (D) are depicted as transparent sticks and balls, the terminal residues involved in ODN binding colored by the element. The GEM91 strand is portrayed as transparent sticks. Each non-covalent interaction (salt-bridges, H-bonds, and π–cation interactions) is highlighted by a dotted black line. Water and ions are omitted for clarity.

Fig. 10C), which justifies the higher efficacy of these dendrimer branches in ODN binding and, consequently, the greater stabilization of the relevant complex with respect to those made from **1** and **2** (Table 4). When this N atom bears a neat, positive charge as in **4**, beside the salt-bridges and some H-bonds, we detect the unsaturation of a number of permanent π–cation interactions involving this quaternary nitrogen and the aromatic rings of the nucleic bases, as shown in Fig. 10D. These interactions are quite strong and, hence, contribute to the higher efficiency of *per residue* (as well as overall) ODN affinity of G2 carbosilane dendrimer **4**.

The free energy analysis described above allows for several, further comments. First, the different lengths of the dendrimer branches between molecules **1** and **3** reflect in a considerably higher efficiency of the latter dendrimer to bind both ODNs: thus, $\Delta G_{bind,eff}/N_{eff}$ = −2.0 and −1.9 kcal mol^{-1} for **1** in complex with GEM91 and SREV while $\Delta G_{bind,eff}/N_{eff}$ = −4.3 and −4.0 kcal mol^{-1} for **3** bound to the same two nucleotide sequences, respectively (Table 4). At the same time, doubling the number of branching – and hence the number of positive charges – in passing from **1** to **2** reflects only in a modest, although not negligible, increase in ODN affinity. That is to say, the architecture of the dendrimer branches rather than the dendrimer overall charge seems to be a fundamental parameter for effective ODN binding in this series of G2 carbosilane dendrimers. Comparing now the performance of dendrimers **2** and **4**, both with the overall charge +16, highlights the importance of another molecular architecture parameter, that is the location of the charges within the molecular structure. In fact, according to the present calculations, having 2 positive charges on the same branch as in **4** (Fig. 1) is far more efficient as concerns ODN binding than having 2 positive charges on two vicinal branches, as in **2** (Fig. 1). Indeed, the architecture of dendrimer **4** allows, aside from the ever-present salt bridges, the realization of other intermolecular dendrimer/ODN contacts such as H-bonds and π–cation interactions (Table 5) within the supermolecular complex. These, in turn, make dendrimer **4** not only dramatically more effective in binding the ODNs with respect to **2** ($\Delta G_{bind,eff}/N_{eff}$ = −2.7 and −2.4 kcal mol^{-1} for **2** in complex with GEM91 and SREV while $\Delta G_{bind,eff}/N_{eff}$ = −5.7 and 5.4 kcal mol^{-1} for **4** in complex with the same ODNs, Table 4), but also make this molecule the best binder of the entire series. Lastly, it is instructive to compare dendrimers **3** and **4**. Indeed, these two molecules present the same molecular architecture but they differ by the number of positive charges (+8 and +16, respectively). Thus, while the tertiary nitrogen atoms characterizing the branches of **3** are involved in a plethora of permanent, stabilizing H-bonds with the nucleic acid bases, making this dendrimer a good ODN binder, the inner quaternary nitrogens of **4** are engaged in several π–cation interactions (Table 5), which decidedly enhance the affinity of these dendrimer branches toward the nucleic acid strand ($\Delta G_{bind,eff}/N_{eff}$ = −4.3 and −4.0 kcal mol^{-1} for **3** bound to GEM91 and SREV and $\Delta G_{bind,eff}/N_{eff}$ = −5.7 and −5.4 kcal mol^{-1} for **4** in complex with the same ODNs).

Conclusions

Insufficient concentrations and very short residence time of the anti-retroviral agents at the cellular and anatomical sites are among the major factors that contribute to the failure of eradicating HIV from reservoirs and the development of multidrug resistance against antiretroviral agents. Gene therapy offers the promise of preventing progressive HIV infection by sustained interference with viral replication in the absence of chronic chemotherapy. Accordingly, gene-targeting strategies are being developed with RNA-based agents, such as ribozymes, antisense oligonucleotides, and small interfering RNA, just to name a few. Yet, to date, gene therapy targeting HIV-1 has not fulfilled its promises and hopes. Nonetheless, there is considerable motivation to be optimistic about its future for HIV-1 therapeutics as analysis of unsuccessful anti-HIV-1 gene therapy studies is providing fundamental insights for improvements. One of the major reasons of such failure resides in the fact that, to reach the therapeutic goal of gene delivery, the use of nanocarriers able to reach the desired population of cells avoiding all biological barriers is ineluctably required.

It is estimated that several hundreds of different nanovectors are in various stages of pre-clinical and clinical development toward regulatory approval in the USA and worldwide. These nano-sized molecular entities have the primary function of transporting the active agent to the target site, performing the multiple biobarrier-avoidance tasks required along the way. To perform these ambitious tasks, however, nanovectors must be carefully designed and engineered to employ several, concurrent strategies to localize preferentially at the target cells, and release its therapeutic payload.

G2 cationic carbosilane dendrimers **1–4** have been shown to hold great potential as gene carriers for HIV-1 treatment both *in vitro* and *in vivo*. In particular, the characterization of ODN binding properties of these dendrimers has highlighted a differential affinity for nucleic acid strands notwithstanding a remarkable similarity in structure and overall charge content of the members of this molecular series. Since the detailed knowledge of structure/activity relationships governing the performance of these nano-objects is the ultimate tool for (i) understanding the reasons of their success/failure and (ii) designing new, more efficient, second generation nanovectors, in this work we aimed at unraveling a molecular rationale for the different ODN binding capacity of four G2 carbosilane dendrimers. To the purpose, we performed a thorough *in silico* characterization of the structural and energetical features of G2 carbosilane dendrimers **1–4**, and their complexes with the two single strands ODN GEM91 and SREV. Our results show that these four dendrimers are all characterized by utterly similar shape and size, independently of their molecular architecture or overall molecular charge, and so are the relevant complexes with the nucleic acids. On the other hand, depending on the molecular architecture and/or the disposition of the positive charges within the molecular scaffold, these molecules display a remarkably different capacity of exploiting their charged groups for binding the negative ODNs in an efficient and productive way. Accordingly, the different ODN binding affinity of dendrimers **1–4** has been rationalized considering the normalized effective binding energy $\Delta G_{bind,eff}/N_{eff}$, *i.e.* the performance of each active individual dendrimer branch directly involved in a binding interaction. We have thus shown that different combinations of charge localization/molecular architecture reflect, upon dendrimer/ODN complex formation, in the intermolecular interaction of different nature and

strength; this, in turn, makes some molecules more efficient ODN binders than others. Furthermore, this study conclusively shows that normalized effective binding energy plays a dominant role among the plethora of critical molecular parameters requiring optimization in the design of efficient nanovectors for gene therapy.

Acknowledgements

COST Action TD0802 is acknowledged for scientific network support. Access to CINECA supercomputers Eurora and Fermi (Bologna, Italy) was granted *via* DILUSO and SYMBIOSI projects (Iscra supercomputing grants to DM and SP).

Notes and references

1 M. L. Ehterige, S. A. Campbell, A. G. Erdman, C. L. Haynes, S. M. Wolf and J. McCullough, *Nanomedicine*, 2013, **9**, 1; E. K.-H. Chow and D. Ho, *Sci. Transl. Med.*, 2013, **5**, 216rv4; R. Lehner, X. Wang, S. Marsh and P. Hunziker, *Nanomedicine*, 2013, **9**, 742; V. J. Venditto and F. C. Szoka Jr., *Adv. Drug Delivery Rev.*, 2013, **65**, 80; R. Duncan and R. Gaspar, *Mol. Pharm.*, 2011, **8**, 2010; B. Y. S. Kim, J. T. Rutka and W. C. W. Chan, *N. Engl. J. Med.*, 2010, **363**, 2434; M. Ferrari, *Nat. Rev. Cancer*, 2005, **5**, 161.

2 A. M. Jhaveri and V. P. Torchilin, *Front. Pharmacol.*, 2014, **5**, 1; J. Nicolas, S. Mura, D. Brambilla, N. Mackievicz and P. Couvreur, *Chem. Soc. Rev.*, 2013, **42**, 1147; B. Godin, E. Tasciotti, X. Liu, R. E. Serda and M. Ferrari, *Acc. Chem. Res.*, 2011, **44**, 979.

3 M. Moros, S. G. Mitchell, V. Grazù and J. M. de la Fuente, *Curr. Med. Chem.*, 2013, **20**, 2759; Q. Sun, M. Radosz and Y. Shen, *J. Controlled Release*, 2012, **164**, 156.

4 S. Svenson, *Mol. Pharm.*, 2013, **10**, 848.

5 C. M. Dawidczyk, C. Kim, J. H. Park, L. M. Russell, K. H. Lee, M. G. Pomper and P. C. Searson, *J. Controlled Release*, 2014, **187C**, 133.

6 S. Y. Wu, G. Lopez Berestein, G. A. Calin and A. K. Socol, *Sci. Transl. Med.*, 2014, **6**, 240ps7; H. Shen and M. Ferrari, *Cancer Gene*, 2012, **19**, 367; J. R. Viola, S. El-Andaloussi, I. I. Oprea and C. L. Smith, *Expert Opin. Drug Deliv.*, 2010, **7**, 721.

7 J. Wu, W. Huang and Z. He, *Sci. World J.*, 2013, 630654; D. Shcharbin, A. Shakhbazau and M. Bryszewska, *Expert Opin. Drug Deliv.*, 2013, **10**, 1687; M. A. Mintzer and M. W. Grinstaff, *Chem. Soc. Rev.*, 2011, **40**, 173.

8 G. Maartens, C. Celum and S. R. Lewin, *Lancet*, 2014, **384**, 258.

9 Y. Deng, C. C. Wang, K. W. Choy, Q. Du, J. Chen, Q. Wang, L. Li, T. K. Chung and T. Tang, *Gene*, 2014, **538**, 217; A. A. Date and C. J. Destache, *Biomaterials*, 2013, **34**, 6202.

10 J. P. Dassie and P. H. Giangrande, *Ther. Delivery*, 2013, **4**, 1527; J. Zhou and J. J. Rossi, *BioDrugs*, 2012, **26**, 393.

11 M. Dirin and J. Winkler, *Expert Opin. Biol. Ther.*, 2013, **13**, 875.

12 A. J. Perisé-Barrios, J. L. Jiménez, A. Domínguez-Soto, F. J. de la Mat, A. L. Corbí, R. Gomez and M. A. Muñoz-Fernandez, *J. Controlled Release*, 2014, **184**, 51; E. Pedziwiatr-Werbicka, E. Fuentes, V. Dzmitruk, J. Sánchez-Nieves, M. Sudas, E. Drozd, A. Shakhbazau, D. Shcharbin, F. J. de la Mata, R. Gomez-Ramirez, M. A. Munoz-Fernandez and M. Bryszewska, *Colloids Surf., B*, 2013, **109**, 183; E. Pedziwiatr-Werbicka, D. Shcharbin, J. Maly, M. Maly, M. Zaborski, B. Gabara, P. Ortega, J. F. de la Mata, R. Gómez, M. A. Muñoz-Fernandez, B. Klajnert and M. Bryszewska, *J. Biomed. Nanotechnol.*, 2012, **8**, 57; E. Pedziwiatr, D. Shcharbin, L. Chonco, P. Ortega, F. J. de la Mata, R. Gómez, B. Klajnert, M. Bryszewska and M. A. Muñoz-Fernandez, *J. Fluoresc.*, 2009, **19**, 267; L. Chonco, J. F. Bermejo-Martín, P. Ortega, D. Shcharbin, E. Pedziwiatr, B. Klajnert, J. F. de la Mata, R. Eritja, R. Gómez, M. Bryszewska and M. A. Muñoz-Fernandez, *Org. Biomol. Chem.*, 2007, **5**, 1886; J. F. Bermejo, P. Ortega, L. L. Chonco, R. Eritja, R. Samaniego, M. Müllner, E. de Jesus, J. F. de la Mata, J. C. Flores, R. Gomez and M. A. Munoz-Fernandez, *Chem. – Eur. J.*, 2007, **13**, 483; P. Ortega, J. F. Bermejo, L. Chonco, E. de Jesus, J. F. de la Mata, G. Fernández, J. C. Flores, R. Gómez, M. J. Serramía and M. A. Munoz-Fernandez, *Eur. J. Inorg. Chem.*, 2006, 1388.

13 D. Shcharbin, E. Pedziwiatr, L. Chonco, J. F. Bermejo-Martín, P. Ortega, F. J. de la Mata, R. Eritja, R. Gómez, B. Klajnert, M. Bryszewska and M. A. Muñoz-Fernandez, *Biomacromolecules*, 2007, **8**, 2059.

14 D. A. Case, V. Babin, J. T. Berryman, R. M. Betz, Q. Cai, D. S. Cerutti, T. E. Cheatham III, T. A. Darden, R. E. Duke, H. Gohlke, A. W. Goetz, S. Gusarov, N. Homeyer, P. Janowski, J. Kaus, I. Kolossváry, A. Kovalenko, T. S. Lee, S. LeGrand, T. Luchko, R. Luo, B. Madej, K. M. Merz, F. Paesani, D. R. Roe, A. Roitberg, C. Sagui, R. Salomon-Ferrer, G. Seabra, C. L. Simmerling, W. Smith, J. Swails, R. C. Walker, J. Wang, R. M. Wolf, X. Wu and P. A. Kollman, *AMBER 14*, University of California, San Francisco, 2014.

15 G. M. Pavan, P. Posocco, A. Tagliabue, M. Maly, M. Malek, A. Danani, E. Ragg, C. V. Catapano and S. Pricl, *Chem. – Eur. J.*, 2010, **16**, 7781.

16 J. Wang, R. M. Wolf, J. W. Caldwell, P. A. Kollman and D. A. Case, *J. Comput. Chem.*, 2004, **25**, 1157.

17 M. W. Schmidt, K. K. Baldridge, J. A. Boatz, S. T. Elbert, M. S. Gordon, J. H. Jensen, S. Koseki, N. Matsunaga, K. A. Nguyen, S. Su, T. L. Windus, M. Dupuis and J. A. Montgomery, *J. Comput. Chem.*, 1993, **14**, 1347; M. S. Gordon and M. W. Schmidt, Advances in electronic structure theory: GAMESS a decade later, in *Elsevier (Ed.) Theory and Applications of Computational Chemistry: the first forty years*, Elsevier, Amsterdam, 2005, pp. 1167–1189.

18 J.-H. Lii and N. L. Allinger, *J. Comput. Chem.*, 1991, **12**, 186.

19 W. L. Jorgensen, J. Chandrasekhar, J. D. Madura, R. W. Impey and M. L. Klein, *J. Chem. Phys.*, 1983, **79**, 926.
20 J.-P. Ryckaert, G. Ciccotti and H. J. C. Berendsen, *J. Comput. Phys.*, 1977, **23**, 327.
21 X. Wu and B. R. Brooks, *Chem. Phys. Lett.*, 2003, **381**, 512.
22 H. J. C. Berendsen, J. P. M. Postma, W. F. van Gunsteren, A. DiNola and J. R. Haak, *J. Chem. Phys.*, 1984, **81**, 3684.
23 T. Darden, D. York and L. Pedersen, *J. Chem. Phys.*, 1993, **98**, 10089.
24 E. Laurini, P. Posocco, M. Fermeglia, D. L. Gibbons, A. Quintas-Cardama and S. Pricl, *Mol. Oncol.*, 2013, **7**, 968; S. Park and K. Schulten, *J. Chem. Phys.*, 2004, **120**, 5946; S. Park, F. Khalili-Araghi, E. Tajkhorshid and K. Schulten, *J. Chem. Phys.*, 2003, **119**, 3559; B. Isralewitz, J. Baudry, J. Gullingsrud, D. Kosztin and K. Schulten, *J. Mol. Graphics Modell.*, 2001, **19**, 13.
25 J. Srinivasan, T. E. Cheatham, P. Cieplak, P. A. Kollman and D. A. Case, *J. Am. Chem. Soc.*, 1998, **120**, 9401.
26 A. Onufriev, D. Bashford and D. A. Case, *J. Phys. Chem. B*, 2000, **104**, 3712.
27 M. Feig, A. Onufriev, M. S. Lee, W. Im, D. A. Case and C. L. Brooks III, *J. Comput. Chem.*, 2004, **25**, 265.
28 P. K. Maiti, T. Cagin, S.-T. Lin and W. A. Goddard III, *Macromolecules*, 2005, **38**, 979; P. K. Maiti, T. Cagin, G. Wang and W. A. Goddard III, *Macromolecules*, 2004, **37**, 6236.
29 G. Rudnick and G. Gaspari, *J. Phys. A: Math. Gen.*, 1986, **4**, L191.
30 D. A. Tomalia, A. M. Naylor and W. A. Goddard III, *Angew. Chem., Int. Ed. Engl.*, 1990, **29**, 138.